



ISSN: 2617-6548

URL: [www.ijirss.com](http://www.ijirss.com)

## Improving electric machine performance through the implementation of the field-oriented control algorithm

 Jasur Abdubannaev<sup>1\*</sup>,  Hai Liang<sup>1</sup>, Zhu Yiwu<sup>1</sup>,  Mansur Khasanov<sup>2</sup>,  Song Kailin<sup>1</sup>

<sup>1</sup>Zhuzhou Jiacheng Science and Technology Development Co. Ltd, 412007 Zhuzhou, Hunan, China

<sup>2</sup>Department of Power Engineering, Jizzakh Polytechnic Institute, 130100 Jizzakh, Uzbekistan.

Corresponding author: Jasur Abdubannaev (Email: [jasur2202@gmail.com](mailto:jasur2202@gmail.com))

### Abstract

The increasing global push for environmentally conscious policies has encouraged many countries to promote the use of electric-powered machinery, leading to a significant surge in the production of electric vehicles (EVs). As more consumers opt for electric vehicles, there is a concurrent demand for greater efficiency to cater to their needs. One of the key challenges electric vehicle manufacturers face is ensuring that electric motors can deliver power swiftly and accurately to achieve desired speeds. This research paper delves into the development of a motor controller for electric vehicles, utilizing the Field Oriented Control (FOC) approach, which includes the flux controller for three-phase PMSM motors. FOC is a popular technique for motor control, known for its ability to provide precise control and practical application. The paper presents an in-depth exploration of the FOC algorithm, breaking down each component to understand how it contributes to controlling electric motors effectively. A detailed model is developed using MATLAB/Simulink, allowing the researchers to simulate various scenarios and evaluate the outcomes. By conducting this analysis, the paper aims to determine which model parameters yield the most accurate results. The study also examines different conditions and compares the accuracy of their results. Following the simulation, the model with the best accuracy parameters is selected for further testing in real-world scenarios. These tests are conducted to validate the simulation results, ensuring that the proposed motor controller design performs as expected under actual driving conditions. The paper's final section discusses the implications of these findings for electric vehicle technology and offers insights into future developments in this rapidly evolving field.

**Keywords:** Electric vehicles, Field-oriented control, Flux controller, Three-phase permanent magnet synchronous motors.

**DOI:** 10.53894/ijirss.v8i2.5429

**Funding:** This study received no specific financial support.

**History: Received:** 3 February 2025 / **Revised:** 6 March 2025 / **Accepted:** 12 March 2025 / **Published:** 14 March 2025

**Copyright:** © 2025 by the authors. This article is an open access article distributed under the terms and conditions of the Creative Commons Attribution (CC BY) license (<https://creativecommons.org/licenses/by/4.0/>).

**Competing Interests:** The authors declare that they have no competing interests.

**Authors' Contributions:** All authors contributed equally to the conception and design of the study. All authors have read and agreed to the published version of the manuscript.

**Transparency:** The authors confirm that the manuscript is an honest, accurate, and transparent account of the study; that no vital features of the study have been omitted; and that any discrepancies from the study as planned have been explained. This study followed all ethical practices during writing.

**Publisher:** Innovative Research Publishing

## 1. Introduction

The electric vehicle (EV) production industry has seen recent developments, making it increasingly appealing to car buyers. Leading EV manufacturers such as Tesla, BYD, and Volkswagen are integrating cutting-edge technologies, thus expanding the market share of EVs [1]. Electric vehicles, as the name suggests, rely on electric motors for propulsion. Thanks to their high efficiency, compact size, fast responsiveness, and suitability for controlling.

Permanent Magnet Synchronous Motors (PMSM) are being widely adopted not only in the transportation industry but also in robotics and other industrial sectors [2]. The physical model of the equivalent converted PMSM motor is depicted in Figure 1.

The primary objective is to effectively control the performance of these motors to meet the driving requirements. Numerous algorithms exist for motor control, each offering unique advantages based on the specific application and nature of the system [3-5]. Traditional control methods often struggle to maintain optimal performance in dynamic driving conditions, lacking adaptability to varying load conditions. This limitation hampers their ability to provide precise speed regulation and torque management required in high-performance applications [6].

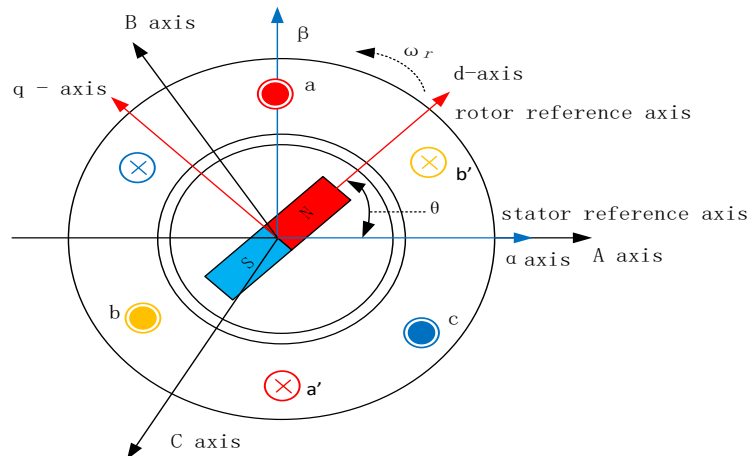


**Figure 1.**  
Physical model of PMSM motor.

In contrast, field-oriented control (FOC) stands out as a preferred method in the EV industry, offering precise motor control and enhanced flexibility to adapt to changing driving scenarios. FOC excels in providing seamless control over electric motors, ensuring smooth acceleration and deceleration, and delivering superior torque control capabilities.

The widespread adoption of FOC can be attributed to its ability to overcome the limitations of traditional control techniques. By leveraging FOC, EVs can achieve improved efficiency and performance across diverse driving conditions, making it the go-to choice for electric vehicle manufacturers.

Analysis and hardware implementation of a sensorless field-oriented control method for permanent magnet synchronous motor drive was investigated in Shrivastava [7] using 3-phase permanent magnet synchronous low-voltage motor control. Addressing practical issues in motor control circuitry, particularly in sensorless permanent magnet synchronous motor control systems for electric vehicle applications, the discussion includes the effects of parasitic elements on insulated gate bipolar transistor-driven inverters, proposing improvements in gate driver circuit topology to mitigate these effects, and verifying the effectiveness of the proposed design through experimental validation, as detailed in Ferdiansyah and Hanamoto [8].

The implementation of vector control methods for speed control of induction motors has been detailed in Manoj [9]. The researchers used a MATLAB-Simulink model to demonstrate improved results with vector control, including reduced rise time, settling time, and peak overshoot. The study also suggests future extensions, such as hardware implementation and the exploration of advanced nonlinear controllers within the Simulink model.

A comparative analysis of Sinusoidal PWM (SPWM) and Space Vector PWM (SVPWM) used in FOC PMSM drives, along with an assessment of their performance under dynamic speed and load disturbance conditions, has been detailed in Jati and Rusli [10] and Pindoriya, et al. [11]. Both results showed that SVPWM exhibited lower torque ripple and coped effectively compared to SPWM under different load conditions. Furthermore, SVPWM maintained a constant speed even with load disturbances, making it a reliable PWM inverter drive for PMSM FOC applications.

The challenge of studying parametric robustness in the control of PMSMs through the application of switched systems theory has been addressed in Nicola, et al. [12]. The study also presents a systematic exploration of stability concepts and the application of these concepts to the control system of a PMSM based on the FOC strategy.

A comprehensive investigation of the effect of resolver eccentricity on the FOC of PMSMs has been presented in Khajuee Zadeh, et al. [13]. It presents an analytical evaluation of the current unbalanced intensity (CUI) caused by resolver position feedback error and proposes an error limit for acceptable operation without motor control derating.

While most types of motor controllers utilize inverters, addressing switching losses is a key consideration during the planning stage. Reference [14] focuses on the design and implementation of an improved gate driver circuit for sensorless

PMSM control, with a specific focus on electric vehicle applications. The study discusses practical issues related to motor control circuits, including the effects of parasitic elements on switching components in the insulated gate bipolar transistor-driven inverter.

One of the biggest issues in the EV production industry is eliminating the initial jerk and improving the response time of the motor controller to reach a steady state. To address these challenges, a modified FOC algorithm [15] has been developed and implemented for PMSM.

In addition to FOC, the Direct Torque Control (DTC) and Model Predictive Control (MPC) methods is also a commonly used technique in motor control. DTC techniques aim to reduce torque ripple, and the cost function is designated based on that objective. Researchers Bao, et al. [16] have presented the integration of the Lyapunov control theory, and the effectiveness of the proposed method has been validated through simulations and experimental results, demonstrating its superior performance in terms of torque ripple reduction and dynamic response. Another research also involves effectively reducing torque ripple while improving current performance. Unlike the presented work in Bao, et al. [16] researchers in Yuan, et al. [17] have used non-parametric predictive current control techniques to overcome torque ripple and current performance challenges.

In order to enable continuous operation in the event of a grid fault, the use of a bi-directional DC-DC converter in an FOC system for PMSM electric drives with a backup supply has been explored [18]. However, the authors only investigated its applicability for low-inertia systems, leaving the question of how to adapt it for high-inertia systems unanswered.

A Fuzzy logic control strategy has been introduced by Kakouche, et al. [19] for multi-power source electric vehicles, utilizing model predictive direct torque control for PMSM traction. The authors achieved a 54.54% improvement over conventional DTC. Authors Djelamda and Bouchareb [20] also use a fuzzy logic control strategy aiming to enhance control accuracy and reduce ripples in motor performance for FOC in PMSM.

However, some exceptions exist where traditional control methods have shown limitations in maintaining optimal performance in dynamic driving conditions, especially in scenarios requiring precise speed regulation and torque management [21]. This underscores the importance of leveraging advanced control techniques like FOC to overcome these challenges and drive efficiency and performance improvements in electric vehicles. This research paper focuses on the implementation of a motor controller for electric vehicles using FOC, a widely utilized technique known for its precise control and practicality, particularly in the context of PMSM. The paper provides a detailed analysis of each component of the algorithm and presents a model developed using MATLAB/Simulink.

The remainder of the paper is structured as follows: Section II explains the methodology, Section III presents the simulation results, Section IV compares the simulation results with real hardware applications, and finally, Section V provides conclusions.

## 2. Methodology

FOC is a precise control method widely used in electric motors to achieve accurate and efficient performance. Its main goal is to minimize the difference between measured and desired motor speeds. Equation (1) describes this objective within the FOC algorithm [22].

$$\max \sum_{t=0}^T \frac{P_{out}(t)}{P_{in}(t)} \tag{1}$$

where  $P_{out}(t)$  and  $P_{in}(t)$  are output (mechanical) and input (electrical) power at instant (t) time, respectively. T is performing time.

However, there are several limitations to consider during FOC implementation. In this methodology section, we will explain the main parts of the FOC algorithm, including how measurements are taken, Clarke and Park transforms, Proportional-Integral (PI) controllers, inverse Clarke and Park transforms, and Space Vector Pulse Width Modulation (SVPWM). By breaking down each part of the FOC algorithm, we aim to provide a clear understanding of how FOC helps control electric motors effectively in different situations.

Field-oriented control derives its name from its fundamental principle of orienting the control of magnetic

fields within electric motors. The primary objective of Field Oriented Control (FOC) is to precisely regulate the magnetic field orientation and magnitude in the motor, enabling accurate control of motor performance. In electric motors, speed is directly proportional to the frequency of the rotating magnetic field [10, 23]. Therefore, by controlling the stator's voltage, FOC effectively governs the creation of the required current (magnetic field) to achieve the desired motor speed.

The governing equations for PMSM are as follows:

$$\begin{cases} V_d = R_s \cdot i_d + L_d \cdot \frac{di_d}{dt} - \omega \cdot L_q \cdot i_q \\ V_q = R_s \cdot i_q + L_q \cdot \frac{di_q}{dt} + \omega \cdot (L_d \cdot i_d + \Psi_m) \\ T_m - T_l = J \cdot \frac{d\omega}{dt}, \quad T_m = N \cdot \Psi_m \cdot i_q \end{cases} \tag{2}$$

where,  $\Psi_m$  - the magnetic flux of the permanent magnet, N - the number of pole pairs,  $\omega$  - the mechanical speed of

the rotor,  $J$  - inertia of the rotor,  $R_s$  - stator resistance,  $L_d$  and  $L_q$  - stator d and q axis inductance respectively.

By focusing on aligning and manipulating the magnetic fields within the motor, FOC ensures that torque production and speed control are optimized for efficient motor operation. This field-oriented approach allows for independent control of the torque-producing magnetic field (flux) and the torque-inducing current, leading to enhanced motor efficiency, improved dynamic response, and precise speed regulation [20]. Figure 2. illustrates a block diagram of the FOC algorithm.

In essence, FOC aims to synchronize and adjust the magnetic fields within electric motors to achieve the desired performance characteristics, emphasizing the importance of controlling the magnetic field orientation and strength to enable accurate speed control and efficient motor operation [24].

2.1. Measuring

To achieve precise control of a motor's speed and behavior, measuring stator current, rotor position, and rotor speed is essential. The required sampling frequency depends on the specific motor type, control strategy, and desired level of precision. While modern electronic devices can reach MHz sampling rates, it is generally accepted that a kHz sampling rate might be sufficient for basic speed control applications, especially considering computational limitations.

Since the measuring signal has a discrete value to reduce the noise and filtering the signal method will be applied before sending the signal. The exponential Weighted Moving Area (EWMA) method is a commonly used technique in signal processing and filtering. It is used to filter out noise from a signal by giving more weight to recent data points while gradually decreasing the influence of older data points [25]. By adjusting the smoothing factor or the weight given to each data point, we can control how much noise is filtered out and how responsive the filter is to changes in the signal.

$$\varepsilon(t) = \alpha \cdot X(t) + (1 - \alpha) \cdot \varepsilon(t - 1) \quad (3)$$

where,  $\varepsilon(t)$  and  $\varepsilon(t - 1)$  - moving average at time t and t-1 respectively.  $\alpha$  - weighting factor,  $\alpha \in [0,1]$ .  $X(t)$  - value of a signal at time t.

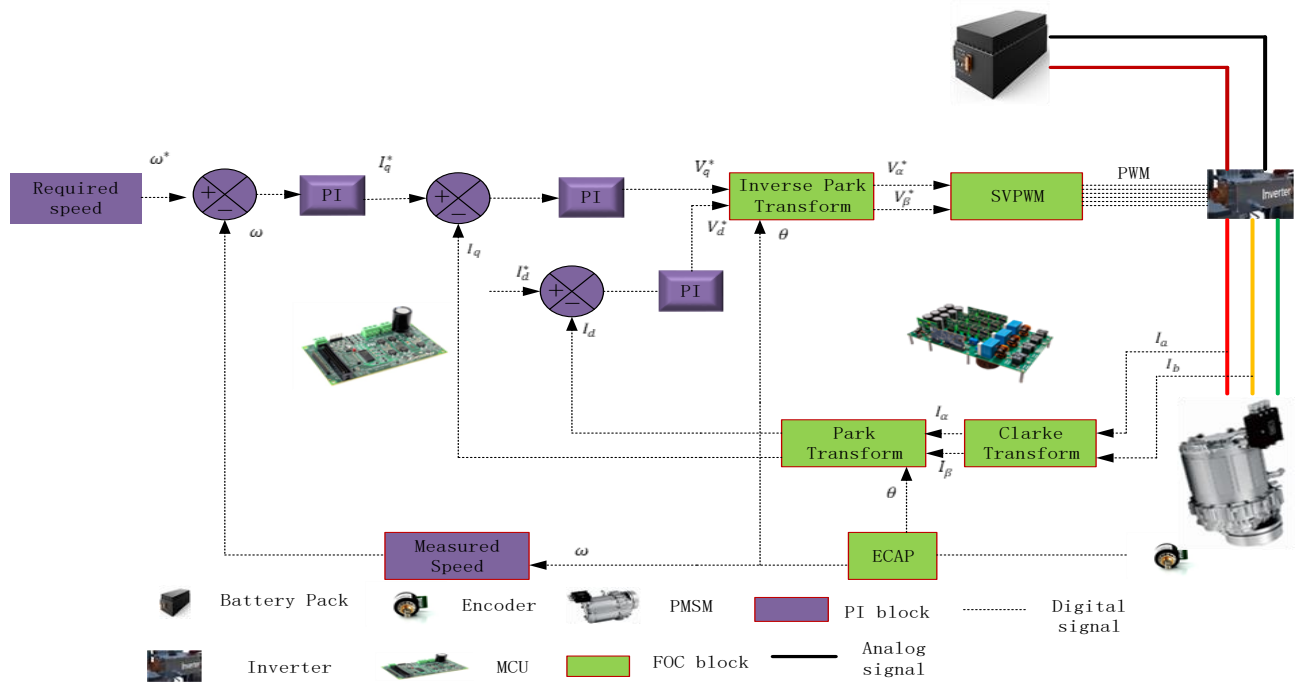
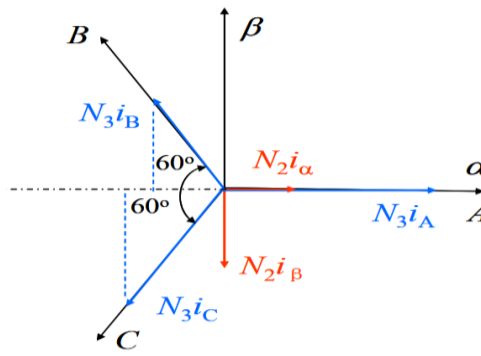


Figure 2. Block diagram of FOC-based PMSM drive system.

2.2. Clarke Transformation

The Clarke transformation helps simplify the analysis and control of three-phase systems by transforming the three-phase variables into a two-dimensional space. This transformation involves mapping the three-phase quantities onto a two-dimensional plane using trigonometric functions. Figure 3 represents the relationship between a three-phase coordinate system (known as ABC) and a two-phase coordinate system (known as  $\alpha\beta$  system).



**Figure 3.**  
The Vector representation of three phase system and system.

After analyzing [Figure 3](#) and knowing the values of the equation are the same before and after converting, we can find  $N_2 = \sqrt{3}$  and  $N_3 = \sqrt{2}$ . Now, we can write the Clarke transform equation as follows:

$$\begin{bmatrix} i_\alpha(t) \\ i_\beta(t) \\ i_0(t) \end{bmatrix} = \frac{\sqrt{2}}{\sqrt{3}} \begin{bmatrix} 1 & -\frac{1}{2} & -\frac{1}{2} \\ 0 & \frac{\sqrt{3}}{2} & -\frac{\sqrt{3}}{2} \\ \frac{1}{\sqrt{3}} & \frac{1}{\sqrt{3}} & \frac{1}{\sqrt{3}} \end{bmatrix} \begin{bmatrix} I_A(t) \\ I_B(t) \\ I_C(t) \end{bmatrix} \quad (4)$$

Since in a balanced system  $I_A(t) + I_B(t) + I_C(t) = 0$  and thus  $I_C(t) = -(I_A(t) + I_B(t))$ .

After replacing the value of  $I_C(t)$  and doing some mathematical computation we can write the above equation in the following form:

$$\begin{bmatrix} i_\alpha(t) \\ i_\beta(t) \end{bmatrix} = \begin{bmatrix} \frac{\sqrt{3}}{2} I_A(t) \\ \frac{\sqrt{2}}{2} I_A(t) + \sqrt{2} I_B(t) \end{bmatrix} \quad (5)$$

So, in this case we only measure two phase currents and convert it to digital signals [\[26\]](#).

### 2.3. Park Transformation

Given that the motor speed aligns with the rotor's electromagnetic field, which is represented by the currents  $I_d$  and  $I_q$ , it becomes necessary to convert the Clarke transformation into the  $I_d$  and  $I_q$  representation. This conversion is commonly known as the park transformation, which allows us to express current and voltage quantities in a two-dimensional rotating reference frame [\[27\]](#). [Figure 4](#) illustrates a visual depiction of the d and q-axis frame of the motor.

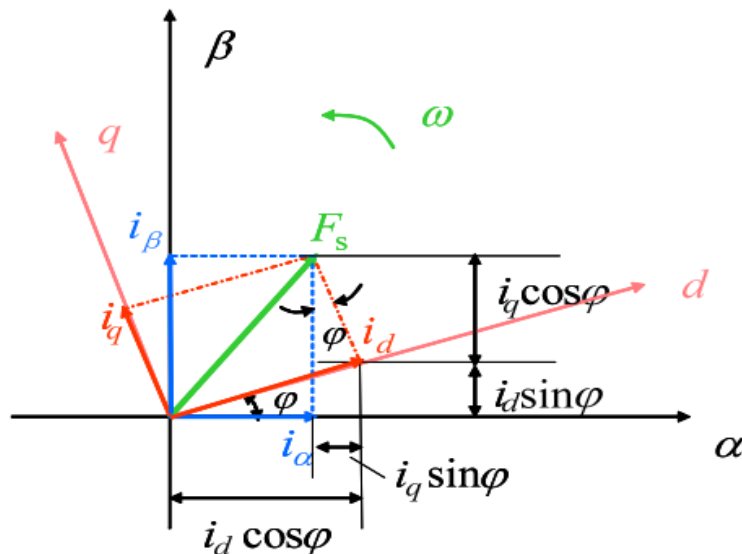


**Figure 4.**  
Graphical representation of d, q axis frame of the motor.

Park transformation form is expressed as the following equation:

$$\begin{bmatrix} i_d \\ i_q \end{bmatrix} = \begin{bmatrix} \cos \theta & \sin \theta \\ -\sin \theta & \cos \theta \end{bmatrix} \begin{bmatrix} i_\alpha \\ i_\beta \end{bmatrix} \quad (6)$$

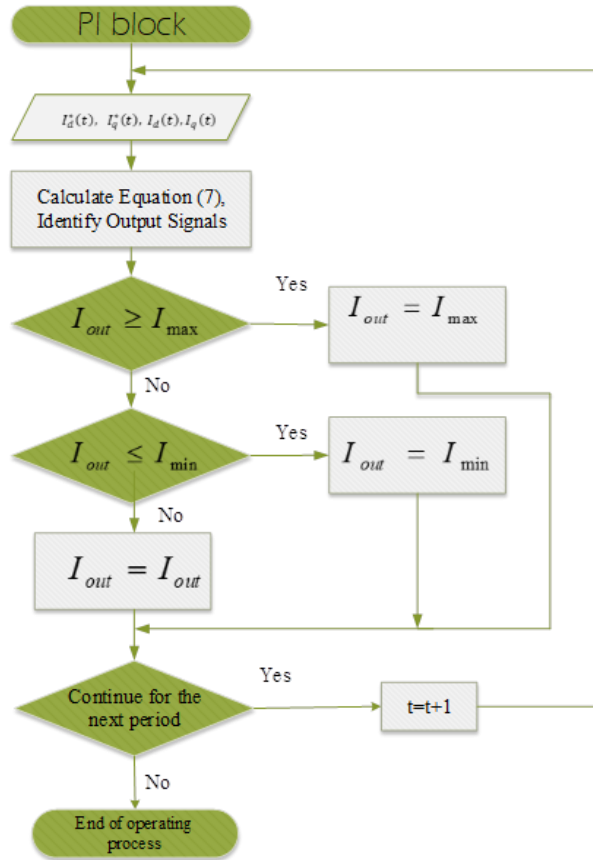


Figure 5. Proposed Algorithm for Limiting Output Signal to Prevent Integral Windup.

2.4. PI Controller

The PI controller is a technique that is applied in various applications and has shown numerous advantages in controlling Permanent Magnet Synchronous Motors (PMSMs) as well. The working principle of a PI controller involves controlling the output value of the controller by comparing the difference between the commanded value and the actual process value [28].

$$\kappa(t) = K_p \cdot e(t) + K_i \cdot \int e(t) d(t) \quad (7)$$

where,  $\kappa(t)$  – PI control variable,  $e(t)$  – error value,  $K_p$  – Proportional Gain Coefficient,  $K_i$  – Integral Gain coefficient.

Since speed is the primary parameter of interest for evaluating the behavior of the PMSM, the PI controller continuously computes the error between the measured speed and the desired speed. It then adjusts the control output based on this error, ensuring that the motor operates at the desired speed with precision and stability [29]. However, in practical scenarios, the integral term of the controller can accumulate excessively beyond the control signal limits, which may lead to overheating and decreased motor efficiency. To address this issue, this paper proposes limiting the output signal. The proposed algorithm is illustrated in Figure 5.

2.5. Inverse Park Transformation

After obtaining the identified values of  $U_d$  and  $U_q$ , the Inverse Park equation is applied to calculate  $U_\alpha$  and  $U_\beta$ . This computation is carried out using (8) [30].

$$\begin{bmatrix} U_\alpha \\ U_\beta \end{bmatrix} = \begin{bmatrix} \cos \theta & -\sin \theta \\ \sin \theta & \cos \theta \end{bmatrix} \begin{bmatrix} U_d \\ U_q \end{bmatrix} \quad (8)$$

2.6. Space Vector Pulse Width Modulation (SVPWM)

To drive electric motors, three-phase, two-level H-bridge converters are the most popular and widely used

applications. Among various control techniques, Space Vector Pulse Width Modulation (SVPWM) stands out as the most advanced method for effectively managing switching states and duty cycles compared to traditional PWM techniques [31]. By predefining vectors, the switching states can be efficiently determined in advance, reducing switching losses. By identifying the sector, the switching states and duty cycles for each state are computed, enabling the generation of PWM signals based on this information. Figure 6 elucidates how SVPWM efficiently synthesizes the desired output voltage by strategically combining the eight switching vectors, resulting in precise control over the motor.

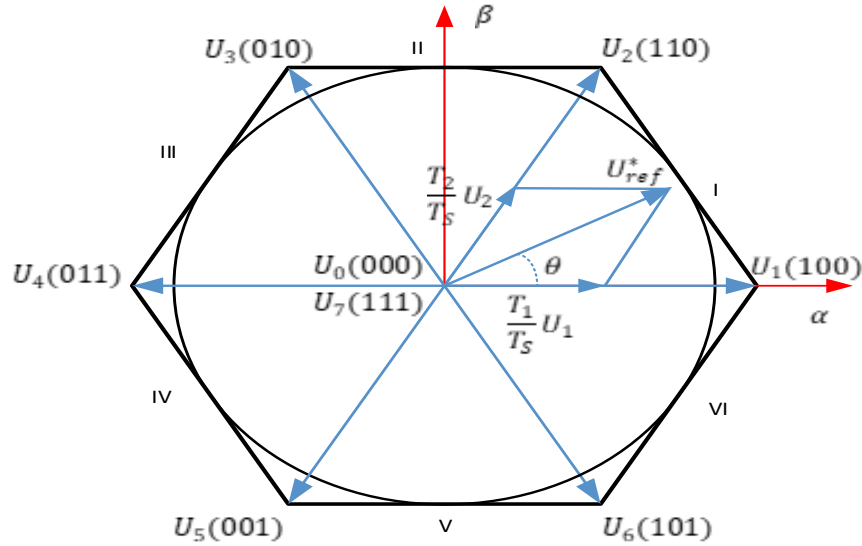


**Figure 6.** Space Vector Pulse Width Modulation (SVPWM) Technique and Switching Vector Combination.

2.6.1. Identifying  $U_\alpha$  And  $U_\beta$  Determine the Sector of the Reference Voltage

The first step in space vector modulation involves identifying the sector where the space voltage vector is determined by  $U_\alpha$  and  $U_\beta$  is located. The typical method of determination entails calculating the magnitude of the voltage vector based on  $U_\alpha$  and  $U_\beta$  then combining the positive and negative values of  $U_\alpha$  and  $U_\beta$ . This method has evident drawbacks, as it incorporates nonlinear functions and trigonometric functions, making it computationally complex, particularly in practical systems. Achieving consistency with this method becomes even more challenging.

Table 1 delineates the sector of the reference voltage  $U_{ref}^*$  based solely on the values of  $U_\alpha$  and  $U_\beta$ . Through this analysis, the table provides insight into how  $U_{ref}^*$  is categorized within specific sectors, aiding in the understanding and implementation of the control algorithm. This method facilitates the computational process and requires less memory space compared to using trigonometric functions [32].

**Table 1.** Sign of  $U_{ref}^*$  in Different Sectors.

| Sector № | Sign of the $U_{ref}^*$   | Sector № | Sign of the $U_{ref}^*$  |
|----------|---|----------|--|
| I        | $U_\beta > 0$ and $\frac{\sqrt{3}}{2}U_\alpha - \frac{1}{2}U_\beta > 0$   | IV       | $U_\beta < 0$ and $\frac{\sqrt{3}}{2}U_\alpha - \frac{1}{2}U_\beta < 0$  |
| II       | $U_\beta > 0$ and $ \frac{\sqrt{3}}{2}U_\alpha  - \frac{1}{2}U_\beta < 0$ | V        | $U_\beta < 0$ and $-\frac{\sqrt{3}}{2}U_\alpha - \frac{1}{2}U_\beta > 0$ |
| III      | $U_\beta > 0$ and $-\frac{\sqrt{3}}{2}U_\alpha - \frac{1}{2}U_\beta > 0$  | VI       | $U_\beta < 0$ and $-\frac{\sqrt{3}}{2}U_\alpha - \frac{1}{2}U_\beta < 0$ |

By applying the above conditions, the interval can be determined using simple addition, subtraction, and logical operations to prevent. This approach eliminates the need for complex nonlinear functions, which is crucial for reducing

computation and enhancing system response speed. However, this expression can be further streamlined for conciseness. Upon further analysis of the aforementioned conditions, the judgment method can be enhanced. Upon simplification, it becomes evident from the derived conditions that the sector containing  $U_{ref}^*$  can be entirely determined by the relationship

between equations  $U_\beta$ ,  $\frac{\sqrt{3}}{2}U_\alpha - \frac{1}{2}U_\beta$ ,  $-\frac{\sqrt{3}}{2}U_\alpha - \frac{1}{2}U_\beta$  and 0. Consequently, the following variables can be defined:

$$U_{ref1} = U_\beta, U_{ref2} = \frac{\sqrt{3}}{2}U_\alpha - \frac{1}{2}U_\beta, U_{ref3} = -\frac{\sqrt{3}}{2}U_\alpha - \frac{1}{2}U_\beta$$

Redefine:

If  $U_{ref1} > 0$  then A = 1, otherwise A = 0

If  $U_{ref2} > 0$  then B = 1, otherwise B = 0

If  $U_{ref3} > 0$  then C = 1, otherwise C = 0

There are eight possible combinations involving A, B, and C, but based on the sector determination formula, A, B, and C are not combined simultaneously. It is either 1 or 0, resulting in six actual combinations with distinct values corresponding to different combinations of A, B, and C. These sectors have a one-to-one correspondence, meaning that the combination of A, B, and C can uniquely determine the sector to which they belong. To differentiate between the six states, let:

$$S = A + 2B + 4C \tag{9}$$

Based on the description provided, it seems that "S" represents six integer values ranging from 1 to 6, which correspond exactly to each of the six sectors. However, there is a distinction between the sequence and the actual order of the sectors, and there exists a corresponding relationship between the numerical value determined by equations (4-9) and the actual sector "N". Table 2 provides redefined sector number after applying above method.

**Table 2.**  
Redefined sector numbers following the application of the proposed method.

| Actual Sector № | I | II | III | IV | V | VI |
|-----------------|---|----|-----|----|---|----|
| Redefine S      | 3 | 1  | 5   | 4  | 6 | 2  |

The process of determining the sector where the reference voltage vector  $U_{ref}^*$  is situated, utilizing the method described above, is exceptionally straightforward as long as it is executed meticulously. When applying a vector, it is crucial to ensure that the calculated S value aligns accurately with the actual sector number N. This alignment helps in precisely identifying the sector in which the reference voltage vector  $U_{ref}^*$  is positioned.

### 2.6.2. Calculate the Action Time $T_x$ , $T_y$ of Adjacent Voltage Space Vectors

After determining the sector where the reference voltage vector  $U_{ref}^*$  is located using the method described above, it is necessary to calculate the parameters. This includes determining the action time of adjacent voltage vectors and corresponding zero vectors in the sector where the voltage vector  $U_{ref}^*$  is situated.

Given the known values of the DC bus voltage  $V_d$  and the sampling period  $T_s$  of the inverter, the action times  $T_x$  and  $T_y$  of adjacent vectors can be determined using the following equations:

$$X = \sqrt{3}U_\beta T_s / V_d \tag{10.1}$$

$$Y = \left( \frac{\sqrt{3}}{2}U_\beta + \frac{3}{2}U_\alpha \right) T_s / V_d \tag{10.2}$$

$$Z = \left( \frac{\sqrt{3}}{2}U_\beta - \frac{3}{2}U_\alpha \right) T_s / V_d \tag{10.3}$$

For different sectors,  $T_x$  and  $T_y$  can be taken as values according to Table 3.

**Table 3.**  
Table of  $T_x$  and  $T_y$  Assignments.

| Sector № | I  | II | III | IV | V  | VI |
|----------|----|----|-----|----|----|----|
| $T_x$    | -Z | Z  | X   | -X | -Y | Y  |
| $T_y$    | X  | Y  | -Y  | Z  | -Z | -X |

2.6.3. Processing of Overmodulation Transient

Despite the theoretical soundness of calculating  $V_d$  and  $V_q$  values, practical application has revealed errors that cause overmodulation. Ignoring overmodulation might harm motor performance and lead to disastrous consequences [33]. The next step is to identify these causes and offer viable solutions.

Our analysis concludes that overmodulation occurs in the following cases:

- Division Calculation and Sector Misidentification:

Algorithms and truncation errors during division calculations can lead to the voltage synthesis vector being incorrectly identified as being in adjacent sectors. Consequently, the voltage vector expansion is decomposed based on the two switch voltage vectors of these adjacent sectors.

- Inverse Park Transform and Calculation Errors:

The algorithm used for computing the inverse Park transform, along with errors from calculating sine and cosine

functions and truncation errors, contributes to deviations in the actual calculated voltage vector components  $V_d$  and  $V_q$ .

- Sector Misidentification in Trajectory Expansion:

The sector containing the actual voltage vector  $U_{ref}^*$  is sometimes mistakenly identified as an adjacent sector. As a result, the expanded sector calculation also falls within this misidentified sector.

We propose an engineering method that involves initially using the conventional approach to calculate  $V_d$  and  $V_q$ . Our proposed algorithm, illustrated in Figure 7, is designed to mitigate overmodulation by addressing sector misidentification and trajectory compression issues effectively.

2.6.4. Calculate the Corresponding Switching Times  $T_{cm1}$ ,  $T_{cm2}$ ,  $T_{cm3}$  for Three-Phase A, B, and C.

The modulation modes of SVPWM are all continuous switch modulation modes. Taking the PWM output waveform of sector I as an example, as shown in Figure 8. The figure includes the waveform of the triangular carrier and three-phase output voltage, as well as the voltage space vector sequence of the sector.  $T_{cm1}$ ,  $T_{cm2}$ , and  $T_{cm3}$  are the three comparison values compared with the triangular wave to generate the PWM waveform. Assuming that the amplitude and period of the triangular carrier are equal, to ensure the duration of each vector, the comparison values should be calculated as follows:

$$T_{cm1} = (T_s - T_x - T_y) / 4 \quad (11.1)$$

$$T_{cm2} = (T_s - T_x - T_y) / 4 + T_x / 2 \quad (11.2)$$

$$T_{cm3} = (T_s - T_x - T_y) / 4 + T_x / 2 + T_y / 2 \quad (11.3)$$

Among them,  $T_x$  and  $T_y$  are the action times of two non-zero vectors.  $T_x$  and  $T_y$  correspond to the action times of different vectors in different sectors, and the specific corresponding vector can be determined by the order of the vectors in each sector. In any sector,  $T_x$  and  $T_y$  corresponds to the time of the non-zero vectors to act. In a carrier cycle, the specific allocation of three comparison values to which phase can be determined by the PWM waveform of each sector,  $T_{cm1}$  should be allocated to the phase with the highest output duty cycle, and  $T_{cm3}$  should be allocated to the phase with the lowest duty cycle. Drawing from the preceding analysis and the PWM waveform characteristics of each sector in continuous switching modulation mode, Table 4 can be constructed.

Table 4.

The assignment table for switching points  $T_{cm1}$ ,  $T_{cm2}$ , and  $T_{cm3}$ .

| Sector №  | I     | II    | III   | IV    | V     | VI    |
|-----------|-------|-------|-------|-------|-------|-------|
| $T_{cm1}$ | $T_a$ | $T_b$ | $T_b$ | $T_c$ | $T_c$ | $T_a$ |
| $T_{cm2}$ | $T_b$ | $T_a$ | $T_c$ | $T_b$ | $T_a$ | $T_c$ |
| $T_{cm3}$ | $T_c$ | $T_c$ | $T_a$ | $T_a$ | $T_b$ | $T_b$ |

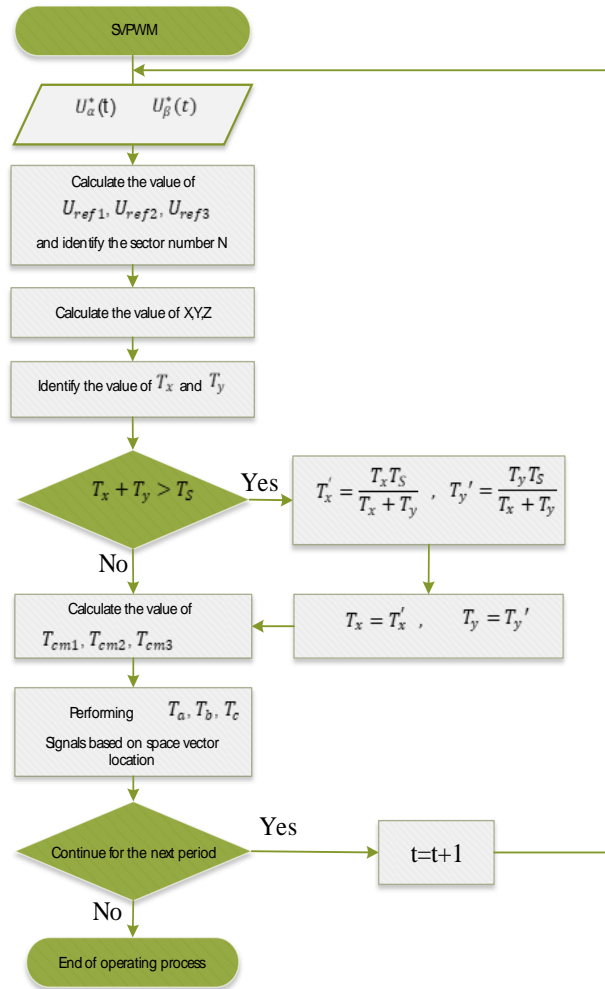


**Figure 7.** The proposed algorithm designed to mitigate overmodulation.

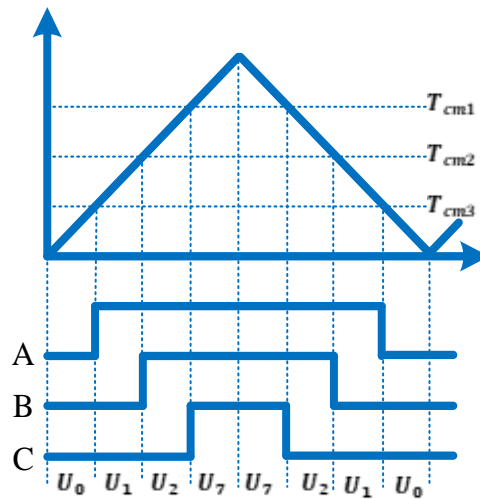


**Figure 8.** The Schematic diagram of SVPWM waveform in sector I.

### 3. Simulation Results.

In this section, a computer simulation was conducted to evaluate the performance of a proposed technique for a permanent magnet synchronous motor (PMSM) based on field-oriented control (FOC). The evaluation was achieved through modeling and testing within the MATLAB/Simulink environment. Figure 9 illustrates the Simulink model, while Table 5 lists the parameters used for the PMSM.

**Table 5.**  
The Parameters of testing model.

| Name of the parameter   | Symbol   | Value                      |
|-------------------------|----------|----------------------------|
| Stator reactance        | $R_s$    | 0.078 Ohm                  |
| Stator $L_d$ inductance | $L_d$    | 0.82 e-3 Ohm               |
| Stator $L_q$ inductance | $L_q$    | 1.28 e-3 Ohm               |
| Number of poles         | $N$      | 5                          |
| Motor Inertia           | $J$      | 1.82 e-4 kg/m <sup>2</sup> |
| Sampling period         | $T_s$    | 100 e-6 sec                |
| Voltage of the DC bus   | $U_{dc}$ | 540 V                      |
| Flux linkage            | $\psi_m$ | 0.3 Wb                     |
| Mechanical torque       | $T_m$    | 250 N·m                    |

The simulation utilized a constant torque test model with a reference speed ramp starting from 477 rpm and reaching a maximum speed of 2000 rpm over a simulation period of 5 seconds. The objective of the simulations was to minimize the objective function (1) while adhering to conditions (2) through (10). Additionally, the impact of coefficients on the low-pass filter was examined, with the motor demonstrating optimal performance when the weighting coefficient  $\alpha$  was set to 0.60.

To evaluate how weighting coefficients  $\alpha$  affect motor efficiency, tests were conducted across various scenarios with differing speeds and torque levels. This testing allowed for the identification of both minimum and maximum motor efficiency values. The findings revealed that motor efficiency fluctuated considerably with changes in torque and speed. Consequently, motor efficiency was assessed based on these observations, and Table 6 illustrates the range of minimum and maximum efficiency values obtained under various EWMA coefficients.

**Table 6.**  
Range of Minimum and Maximum Motor Efficiency Values for Various EWMA Coefficients.

| $N_2$ | $\alpha$ | Min (%) | Max (%) | $N_2$ | $\alpha$ | Min (%) | Max (%) |
|-------|----------|---------|---------|-------|----------|---------|---------|
| 1     | 0.3      | 67      | 90      | 5     | 0.7      | 71      | 93      |
| 2     | 0.4      | 68      | 91      | 6     | 0.8      | 70      | 93      |
| 3     | 0.5      | 70      | 92      | 7     | 0.9      | 69      | 90      |
| 4     | 0.6      | 73      | 96      | 8     | 1        | 68      | 89      |

Figure 10. Exhibits the graphical representations detailing the applied direct and quadratic rotor voltages, denoted as  $V_d$  and  $V_q$  respectively.

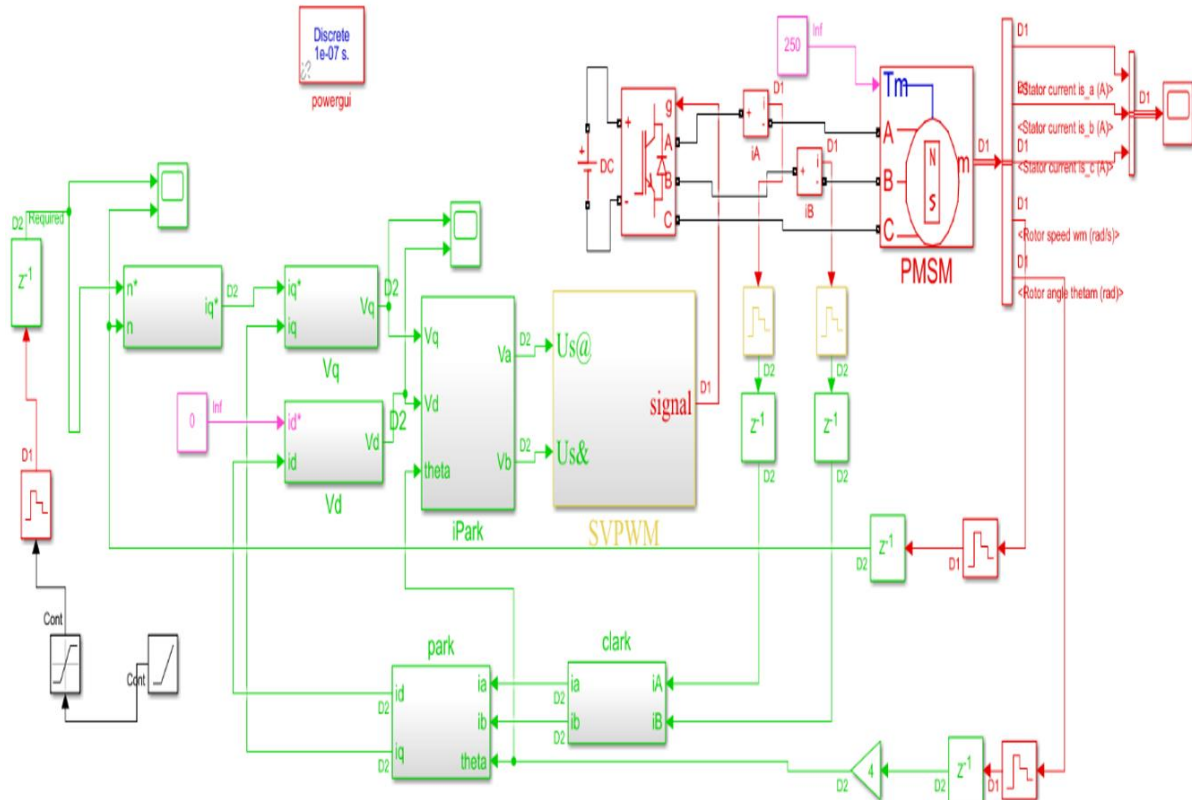


**Figure 9.**  
The Implementation of the FOC algorithm in MATLAB/Simulink.

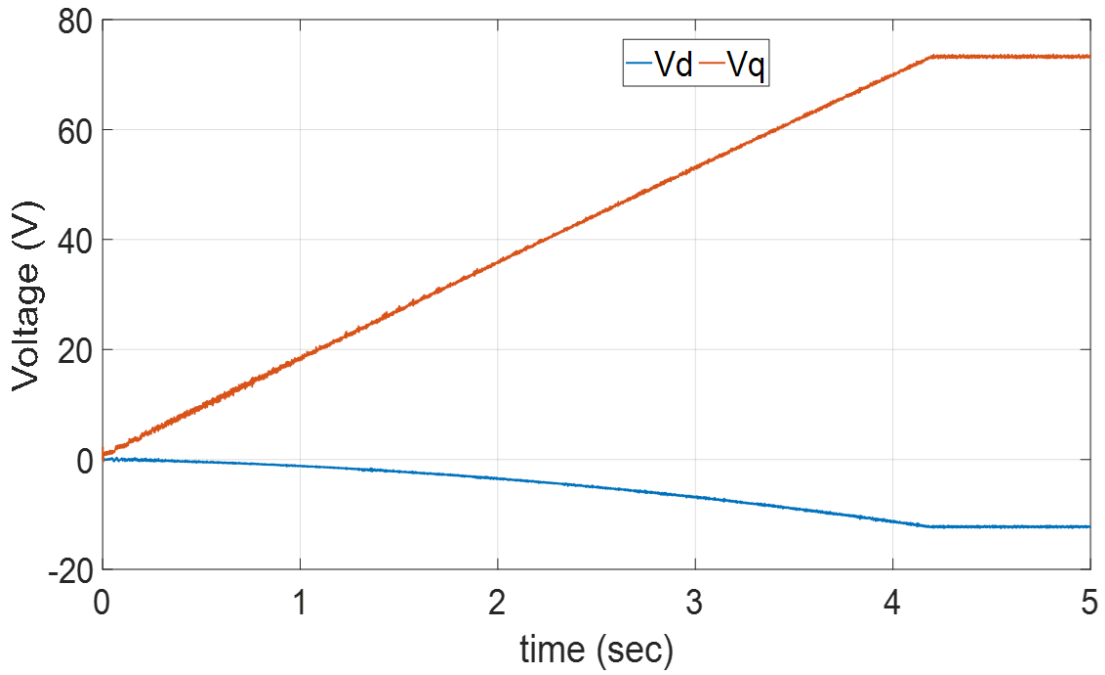


**Figure 10.**  
The Applied direct and quadratic voltages.

Moving forward to [Figure 11](#), a comprehensive illustration outlines the correlation between the reference speed and the corresponding measured speed. Furthermore In [Figure 12](#), the graphical depiction extends to showcase the three-phase stator currents.

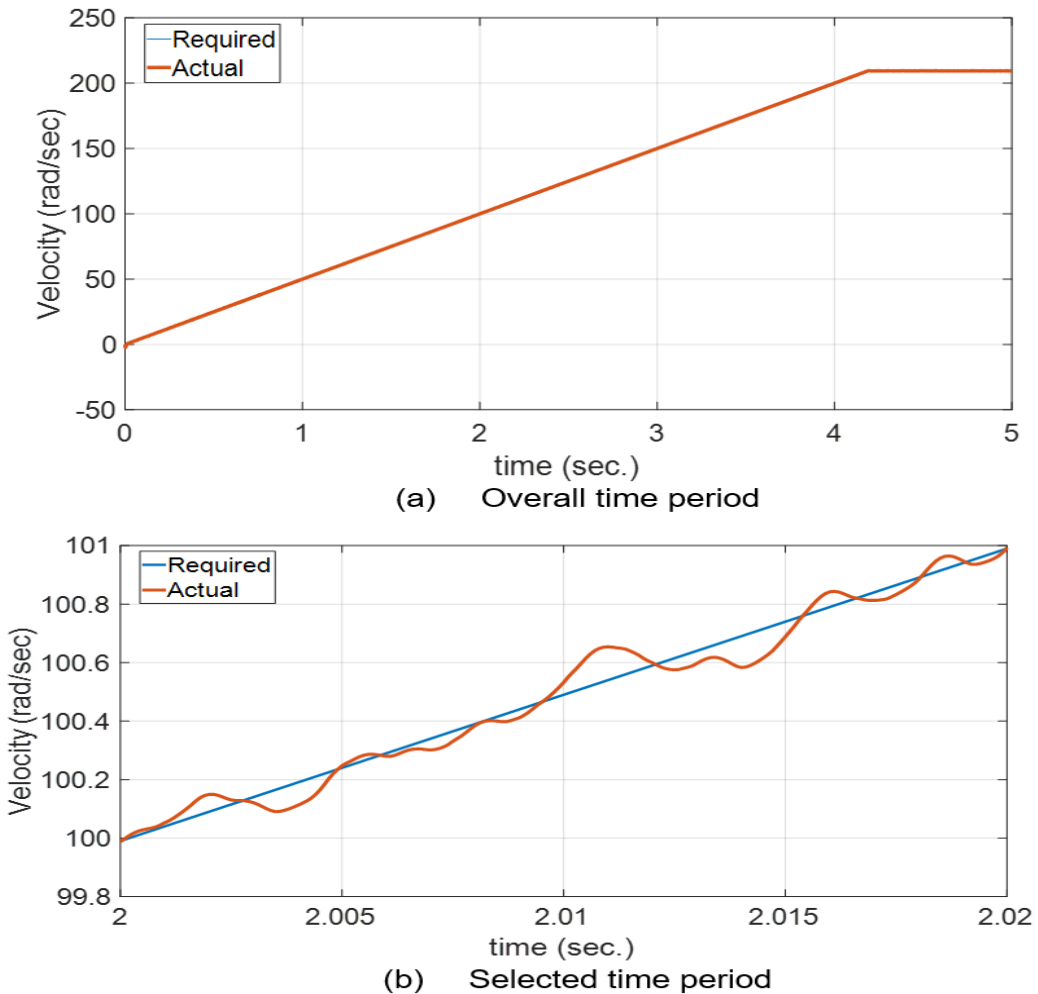
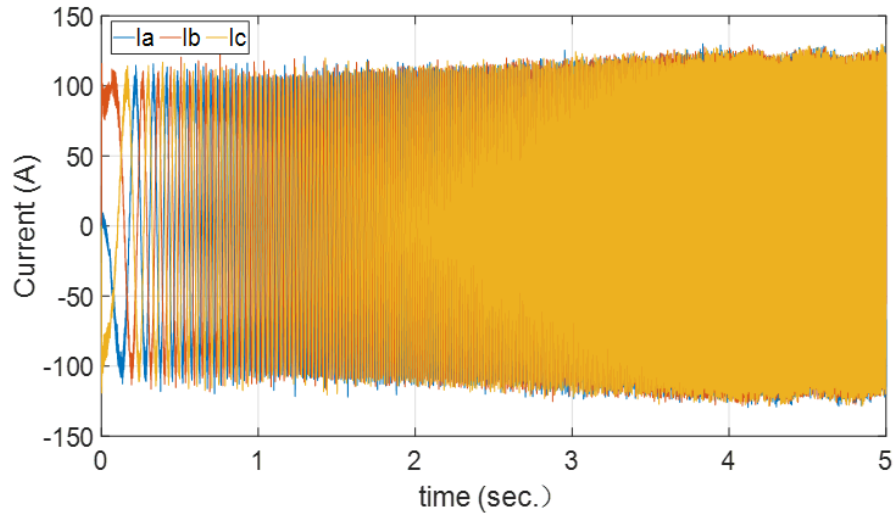
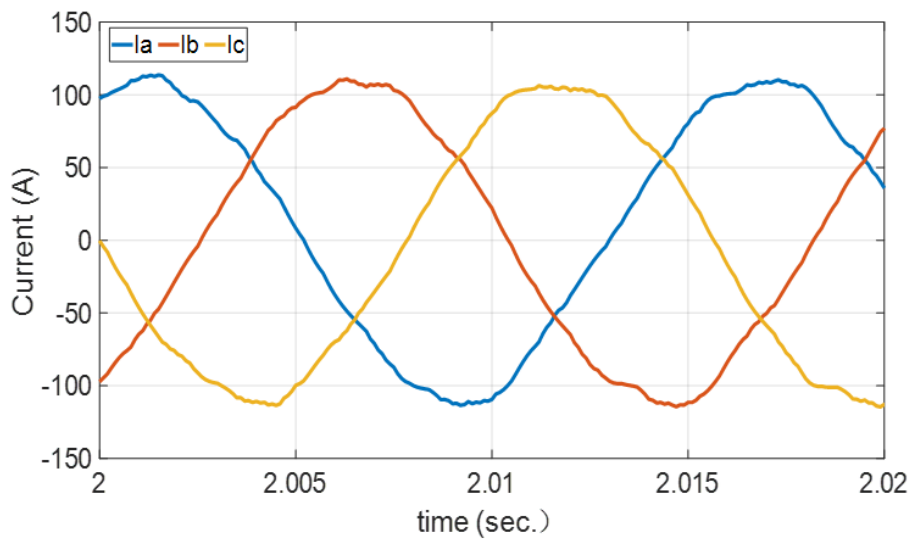


**Figure 11.**  
Characteristics of Actual and required speed over the period.



(a) Overall time period



(b) Selected time period

Figure 12. Three-phase stator output current characteristics.

#### 4. Hardware Experimental Results

The laboratory at "Zhuzhou Jiacheng Science and Technology Co. Ltd." conducted real-time experiments in their New Energy R&D department. Figure 13 illustrates the components of the real test system. The setup involved connecting a three-phase Permanent Magnet Synchronous Motor (PMSM) to a three-phase inverter, with control implemented using an STM32F407 microcontroller. The inverter board was powered by a 24-volt supply. Additionally, a DC generator served as the load for the PMSM. The motor's parameters, as listed in Table 6 of the experimental documentation, were utilized. Decoupled controllers were employed to independently regulate the motor's speed and flux. The speed controller had gains of  $K_P = 0.10801$  and  $K_i = 0.0933$ , and this setup allowed for controlled testing and evaluation of the PMSM's performance under various conditions. The real-time results have also shown that due to the ignorance of the heating factor in the mathematical modeling in Section II, it is required to keep the motor and controller under  $T \leq 140^\circ\text{C}$  and  $T \leq 80^\circ\text{C}$  for stable motor operation.

Figure 14 illustrates the efficiency comparison between the Modified FOC and Non-Modified FOC algorithms under two operational modes: Constant Speed with Torque Variation and Constant Torque with Speed Variation. The results demonstrate that the Modified FOC algorithm consistently achieves higher efficiency compared to the Non-Modified FOC algorithm in both modes.



**Figure 13.**  
The Practical Test System Implementation.

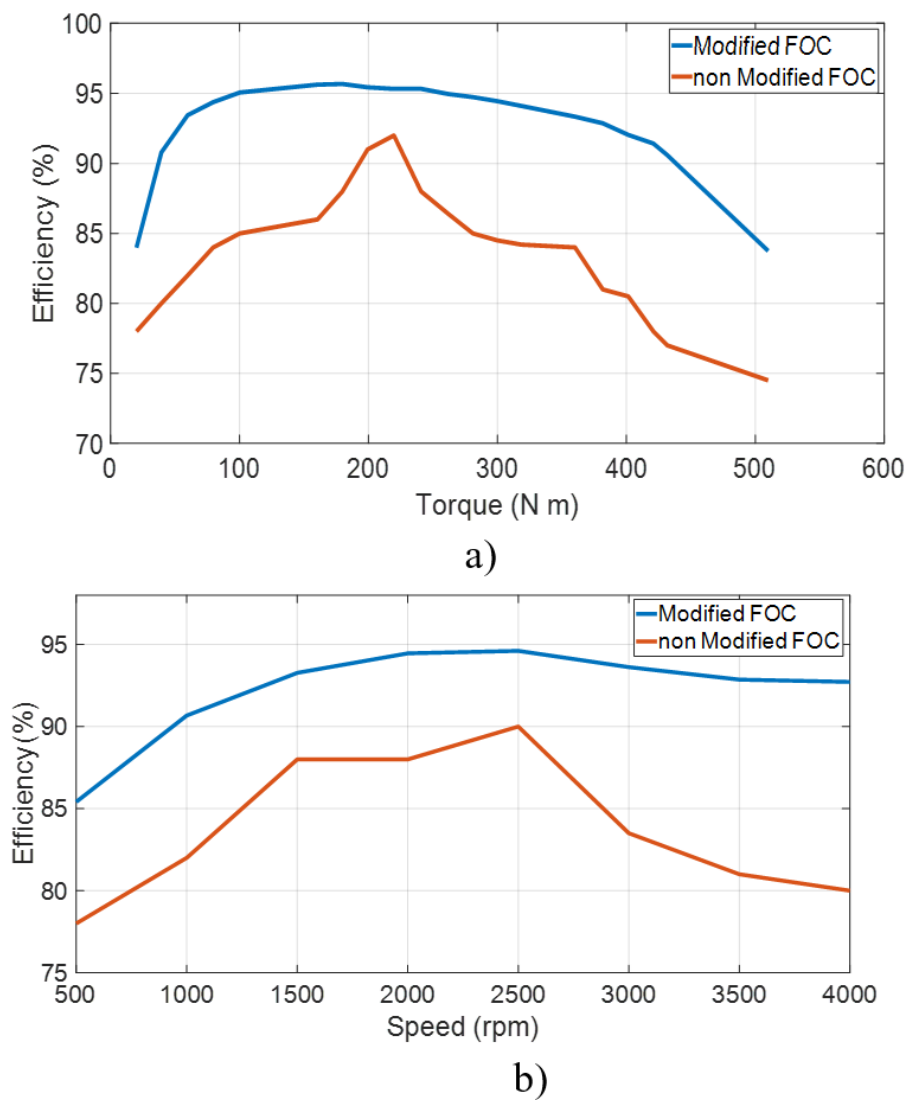


**Figure 14.**  
Performance Analysis of Modified vs. Non-Modified FOC: (a) Constant Torque Speed Variation and (b) Constant Speed Torque Variation.

In detail, the analysis reveals that in the Constant Speed with Torque Variation mode, the Modified FOC algorithm exhibits superior efficiency, particularly as the motor approaches its rated value. Similarly, in the Constant Torque with

Speed Variation mode, the Modified FOC algorithm outperforms the Non-Modified FOC, with maximum efficiency attained when the motor operates at its rated value.

Figure 15 shows the torque variation with voltage and velocity based on the real test experimental results. It is evident that achieving higher speed and torque necessitates the application of higher voltage. However, as torque and speed are inversely proportional, it is vital to identify the range in which the motor system attains its peak performance.

Figure 16 presents graphs of efficiency functions: (a) for the electrical characteristics and (b) for the feed characteristics of the proposed algorithm. The motor system's efficiency is dependent on both the motor control unit's efficiency and the three-phase PMSM. This depiction provides valuable insight into the overall performance and efficiency of the motor system under the proposed algorithm. The motor performance analysis covers speed, torque, power, and efficiency, evaluated through four distinct testing methods. The results—Electric Peak, Feed Peak, Electrical Rated, and Feed Rated—are illustrated in Figures. 17a, 17b, 17c, and 17d, respectively. Each graph displays motor speed on the X-axis, with torque on the left Y-axis and output power along with efficiency on the right Y-axis, providing a comprehensive view of the motor's performance under various conditions.

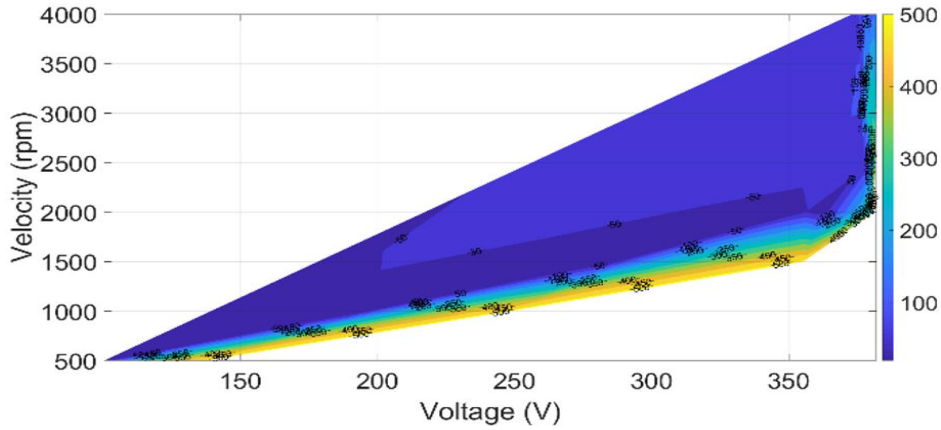


Figure 15  
Torque Variation with Voltage and Velocity.

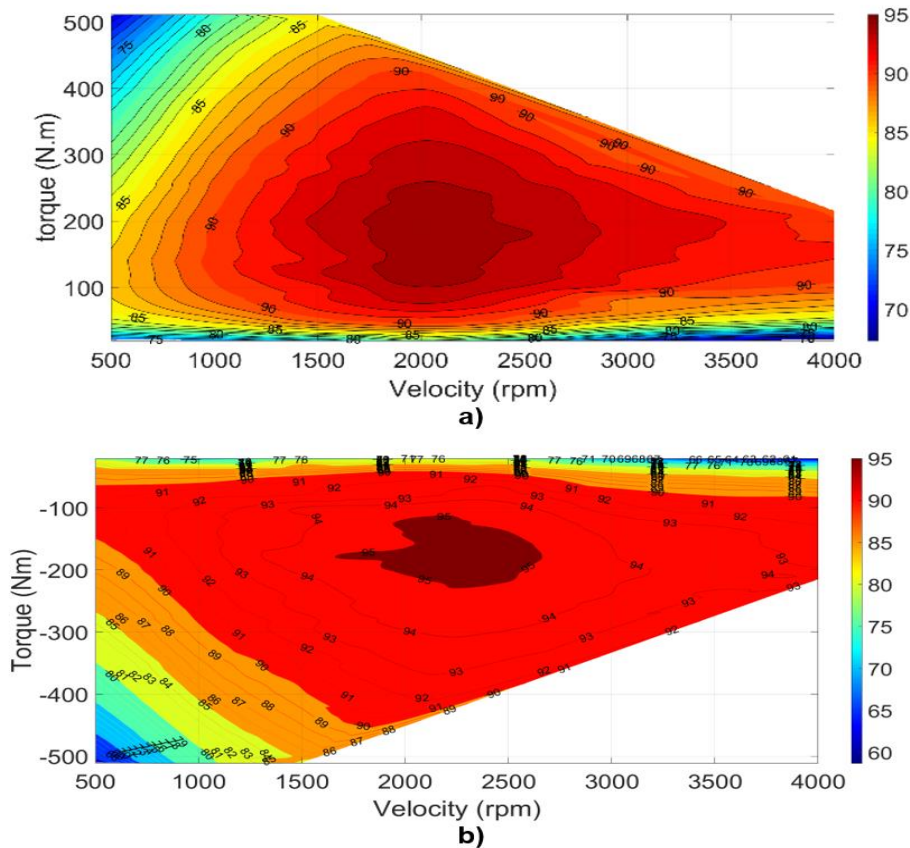
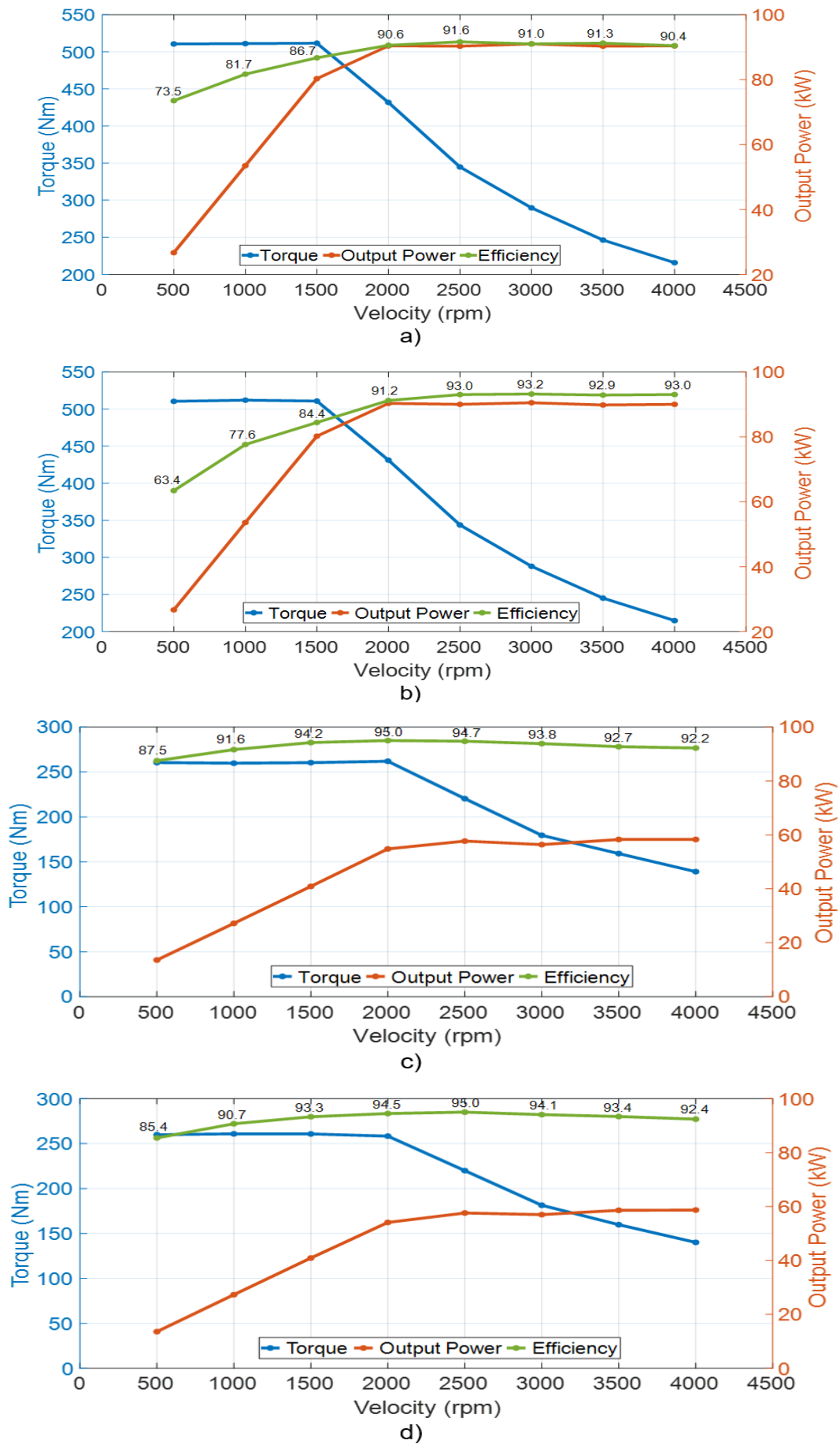


Figure 16.  
Motor System Efficiency Function a) Electrical characteristic b) Feed characteristic



**Figure 17.** The motor performance analysis a) Electric Peak b) Feed Peak c) Electrical Rated d) Feed Rated

## 5. Conclusion

In summary, this study focused on the design and implementation of a field-oriented control algorithm for driving a three-phase PMSM. Through extensive testing in MATLAB/Simulink, various speed characterization scenarios under constant torque and speed conditions were examined. The application of direct and quadratic voltage, along with the comparison of actual speed with reference speed and analysis of switching states of the upper leg of the three-phase inverters and three-phase stator currents, was detailed in Section III. The obtained results were rigorously compared with real-world data, demonstrating that the proposed algorithm significantly enhanced motor performance. By achieving high precision control, the algorithm offers a reliable solution for optimizing electric motor operation. These findings underscore the potential of the proposed algorithm to effectively control PMSMs in practical applications, paving the way for advancements in electric motor technology.

## References

- [1] International Energy Agency's (IEA), "Global EV outlook," Retrieved: <https://www.iea.org/reports/global-ev-outlook-2024/trends-in-electric-cars>, 2024.
- [2] J. Staszak, K. Ludwinek, Z. Gawęcki, J. Kurkiewicz, T. Bekier, and M. Jaśkiewicz, "Utilization of permanent magnet synchronous motors in industrial robots," presented at the 2015 International Conference on Information and Digital Technologies, Zilina, Slovakia, 2015.
- [3] Y. Peng and H. Xiong, "Research on vector control system of permanent magnet synchronous motor based on active disturbance rejection control," presented at the 2023 9th International Conference on Control Science and Systems Engineering (ICCSSE), Shenzhen, China, 2023.
- [4] Y. Li, P. Zhang, J. Hang, S. Ding, L. Liu, and Q. Wang, "Comparison of dynamic characteristics of field oriented control and model predictive control for permanent magnet synchronous motor," *2018 13th IEEE Conference on Industrial Electronics and Applications (ICIEA)*, Wuhan, China, pp. 2431-2434, 2018. <https://doi.org/10.1109/ICIEA.2018.8398117>
- [5] L. Ling, S. D. Huang, G. Z. Cao, and H. Qiu, "Comparison analysis on control-increment-based and control-quantity-based predictive controls of permanent magnet synchronous motors," presented at the 2023 IEEE International Conference on Predictive Control of Electrical Drives and Power Electronics (PRECEDE), Wuhan, China, 2023.
- [6] Y. Li, Z. Ping, Y. Huang, and J. G. Lu, "An internal model approach for speed tracking control of PMSM driven electric vehicle," presented at the 2020 IEEE 16th International Conference on Control & Automation (ICCA), Singapore, 2020.
- [7] R. Shriwastava, "Sensorless field-oriented control of PMSM drive system for automotive application," *International Journal of Electric and Hybrid Vehicles*, vol. 8, no. 3, pp. 213-224, 2016. <https://doi.org/10.1109/ICETET.2015.11>
- [8] I. Ferdiansyah and T. Hanamoto, "Design and implementation of improved gate driver circuit for sensorless permanent magnet synchronous motor control," *World Electric Vehicle Journal*, vol. 15, no. 3, p. 106, 2024. <https://doi.org/10.3390/wevj15030106>
- [9] V. Manoj, "Speed control of induction motor using vector control," *International Journal of Emerging Trends in Engineering and Development*, vol. 4, pp. 336-348, 2023.
- [10] M. P. Jati and M. R. Rusli, "Performance evaluation of SPWM and SVPWM inverter in FOC-based PMSM drives under dynamic speed and load disturbance," in *Proceedings of the 4th Borobudur International Symposium on Science and Technology 2022 (BIS-STE 2022)*, Springer Nature, 2023, vol. 225, p. 182.
- [11] R. M. Pindoriya, B. S. Rajpurohit, and R. Kumar, "A novel application of harmonics spread spectrum technique for acoustic noise and vibration reduction of PMSM drive," *IEEE Access*, vol. 8, pp. 103273-103284, 2020. <https://doi.org/10.1109/ACCESS.2020.2999336>
- [12] M. Nicola, C.-I. Nicola, D. Selişteanu, and C. Ionete, "Control of PMSM based on switched systems and field-oriented control strategy," *Automation*, vol. 3, no. 4, pp. 646-673, 2022. <https://doi.org/10.3390/automation3040033>
- [13] M. Khajuee Zadeh, M. Emadaleslami, F. Tootoonchian, A. Daniar, M. Gardner, and B. Akin, "Comprehensive investigation of the resolver's eccentricity effect on the field-oriented control of PMSM," *IEEE Sensors Journal*, vol. 23, no. 17, pp. 19145-19152, 2023. <https://doi.org/10.1109/JSEN.2023.3292896>
- [14] I. Ferdiansyah and T. Hanamoto, "Design and implementation of an effective motor control devices by improvement gate driver circuit for Pmsm Sensorless Motor Control Application," Retrieved: file:///C:/Users/Ahmadpc/Downloads/preprints202312.0624.v1.pdf. [Accessed 2023].
- [15] P. Ramesh, M. Umavathi, C. Bharatiraja, G. Ramanathan, and S. Athikkal, "Development of a PMSM motor field-oriented control algorithm for electrical vehicles," *Materials Today: Proceedings*, vol. 65, pp. 176-187, 2022. <https://doi.org/10.1016/j.matpr.2022.06.080>
- [16] G. Bao, W. Qi, and T. He, "Direct torque control of PMSM with modified finite set model predictive control," *Energies*, vol. 13, no. 1, p. 234, 2020. <https://doi.org/10.3390/en13010234>
- [17] X. Yuan, S. Zhang, and C. Zhang, "Nonparametric predictive current control for PMSM," *IEEE Transactions on Power Electronics*, vol. 35, no. 9, pp. 9332-9341, 2020. <https://doi.org/10.1109/TPEL.2020.2970173>
- [18] M. Bobrov and A. Shashunkin, "Field oriented control of PMSM drive with backup power supply," *Nexo Revista Cientifica*, vol. 34, no. 04, pp. 1282-1289, 2021. <https://doi.org/10.5377/nexo.v34i04.12664>
- [19] K. Kakouche *et al.*, "Model predictive direct torque control and fuzzy logic energy management for multi power source electric vehicles," *Sensors*, vol. 22, no. 15, p. 5669, 2022. <https://doi.org/10.3390/s22155669>
- [20] I. Djelamda and I. Boucharab, "Field-oriented control based on adaptive neuro-fuzzy inference system for PMSM dedicated to electric vehicle," *Bulletin of Electrical Engineering and Informatics*, vol. 11, no. 4, pp. 1892-1901, 2022. <https://doi.org/10.11591/eei.v11i4.3818>
- [21] S. Liu, C. Liu, Y. Huang, and H. Zhao, "Model predictive two-target current control for OW-PMSM," *IEEE Transactions on Power Electronics*, vol. 36, no. 3, pp. 3224-3235, 2020. <https://doi.org/10.1109/TPEL.2020.3016714>
- [22] W. A. A. Salem and G. F. Osman, & Arfa, S. H., "Adaptive neuro-fuzzy inference system based field oriented control of PMSM & speed estimation," presented at the 2018 Twentieth International Middle East Power Systems Conference (MEPCON), IEEE., 2018.

- [23] H. Ghanayem, M. Alathamneh, and R. Nelms, "PMSM field-oriented control with independent speed and flux controllers for continuous operation under open-circuit fault at light load conditions," *Energies*, vol. 17, no. 3, p. 593, 2024. <https://doi.org/10.3390/en17030593>
- [24] M. P. Jati, M. R. Rusli, Y. C. Manie, and P.-C. Peng, "A speed estimation for reliable performance of field oriented PMSM control using adaptive neuro-fuzzy inference system," in *2023 International Conference on Consumer Electronics-Taiwan (ICCE-Taiwan)*, IEEE, 2023, pp. 373-374.
- [25] S. Hansun and S. Subanar, "Brown's weighted exponential moving average implementation in forex forecasting," *Telecommunication Computing Electronics and Control*, vol. 15, no. 3, pp. 1425-1432, 2017. <https://doi.org/10.12928/TELKOMNIKA.v15i3.5410>
- [26] D. Bellan, "Clarke transformation solution of asymmetrical transients in three-phase circuits," *Energies*, vol. 13, no. 19, p. 5231, 2020. <https://doi.org/10.3390/en13195231>
- [27] R. Madnani and M. K. Mishra, "A visual understanding of electrical transformations and generalized abc to  $\alpha\beta 0$  and dq0 transformation," *International Journal of Circuit Theory and Applications*, vol. 51, no. 2, pp. 963-978, 2023. <https://doi.org/10.1002/cta.3439>
- [28] B. Sarsembayev, K. Suleimenov, and T. D. Do, "High order disturbance observer based PI-PI control system with tracking anti-windup technique for improvement of transient performance of PMSM," *IEEE Access*, vol. 9, pp. 66323-66334, 2021. <https://doi.org/10.1109/ACCESS.2021.3074661>
- [29] I. Qureshi and V. Sharma, "PMSM motor drive and their control schemes," *Journal of Applied Research and Technology*, vol. 22, no. 2, pp. 274-283, 2024. <https://doi.org/10.22201/icat.24486736e.2024.22.2.2321>
- [30] B. Bariya, "Indirect field oriented control of induction motor," *Journal of Electrical Systems*, vol. 20, pp. 2013-2021, 2024. <https://doi.org/10.52783/jes.1793>
- [31] N. D. Irimia, F. I. Lazar, and M. Luchian, "Comparison between sinusoidal and space vector modulation techniques on the resulting electromagnetic torque ripple produced by a three-phase BLDC motor under field-oriented control," presented at the 2019 6th International Conference on Control, Decision and Information Technologies (CoDIT), Paris, France, 2019.
- [32] S. Skoulaxinos, P. Wheeler, and G. Vakil, "Active noise control by means of high frequency injection in electric motors," *IET Electric Power Applications*, vol. 18, no. 8, pp. 897-911, 2024. <https://doi.org/10.1049/elp2.12442>
- [33] S. Liu, C. Liu, Y. Huang, and Y. Xiao, "Direct modulation pattern control for dual three-phase PMSM drive system," *IEEE Transactions on Industrial Electronics*, vol. 69, no. 1, pp. 110-120, 2021. <https://doi.org/10.1109/TIE.2021.3053880>